Journal of Industrial and Engineering Chemistry 36 (2016) 44–48

Contents lists available at ScienceDirect

Journal of Industrial and Engineering Chemistry

journal homepage: www.elsevier.com/locate/jiec

Enhancement in performance of polymer solar cells by introducing solution-processed dipole interlayer

Jae Pil Han, Eui Jin Lee, Yong Woon Han, Tae Ho Lee, Doo Kyung Moon *

Department of Materials Chemistry and Engineering, Konkuk University, 1 Hwayang-dong, Gwangjin-gu, Seoul 05029, Republic of Korea

ARTICLE INFO

Article history:
Received 25 September 2015
Received in revised form 12 November 2015
Accepted 14 November 2015
Available online 28 November 2015

Keywords:
Inverted solar cells
Tunneling effect
Dipole layer
Metal fluoride

ABSTRACT

Metal fluorides (e.g., LiF and BaF_2) are usually introduced as an electron transport layer in conventional polymer solar cells (PSCs). However, because they are insoluble, vacuum deposition is inevitable, resulting in a high process cost and the difficulty of introduction in PSCs. In this study, we fabricated inverted PSCs with a double interlayer by using solution-processable cesium fluoride and ZnO to improve the electron extraction. The power conversion efficiency was enhanced from 7.5% to 8.2% by a 9.3% increase in the fill factor. In addition, we demonstrated the enhancement of the FF by atomic force microscopy, space charge limited current, and photoluminescence.

Introduction

Bulk heterojunction (BHJ) polymer solar cells (PSCs) have attracted considerable attention because of their flexibility, lightness, easy fabrication, and suitability for large-scale and low-cost solution processes. Recently, they achieved a power conversion efficiency (PCE) over 10% in a single structure with the addition of processing additives [1–4] and the introduction of an interlayer [5–7]. However, to commercialize these PSCs, research must be conducted regarding the improvement of their lifespan. In the photoactive layer of the PSCs in a conventional-structure, the BHJ is formed by the electron donor 'D-A type polymer' and electron acceptor 'fullerene-derivative' [8]. This photoactive layer is situated between a poly (3,4-ethylenedioxythiophene):poly(styrene sulfonate)(PEDOT:PSS)-coated indium tin oxide (ITO) anode and a metal cathode with a low work function. However, because of the acidic and hygroscopic characteristics of PEDOT:PSS, ITO electrodes corrode. Moreover, the metal electrode with a low work function easily oxidizes in air, resulting in the decrease of device stability. Therefore, the power conversion efficiency (PCE) decreases [6,9].

To compensate for these disadvantages, there have been many recent studies on inverted-structures. In such a structure, as shown in Fig. 1(a), a photoactive layer is positioned between an ITO cathode coated with metal oxide (e.g., ZnO or TiO_X) or polyelectrolyte and a metal anode with a high work function. PEDOT:PSS is not used in this structure. Because of the metal electrode with a high work function, self-encapsulation occurs. Therefore, inverted-structure exhibits superior long-term stability compared with conventional structures [10–14]. Regarding the photoactive layer, which is usually formed by spin-coating, a donor polymer with a relatively low surface energy is situated in the upper part of the layer, and a fullerene acceptor with a relatively high surface energy is positioned in the lower section [15]. This type of vertical phase separation has a direction opposite to the movement of the electric charge in a conventional structure, which is not ideal. In contrast, for an inverted structure, the PCE can be enhanced by taking advantage of this vertical phase separation [14,15]. Using the active layer of poly{thieno[3,4-b]-thiophene/benzodithiophene} (PTB7):[6,6]-phenyl C_{71} butyric acid methyl ester ($PC_{71}BM$), Cao et al. [14] reported PCEs of 8.24% and 9.2% in conventional and inverted structures, respectively. So et al. [10] reported PCEs of 4.9% and 5.8% in conventional and inverted structures, respectively.

Another typical material for electron-transport layers (ETLs) is metal fluoride (e.g., LiF, BaF_2). If this material is thin enough for an electron to pass through the gap between the cathode and active layer, band bending occurs. Consequently, the energy barrier between the cathode and active layer decreases, and electrons move efficiently owing to the tunneling effects [16–18]. Lee et al. [16] reported the improvement of the efficiency from 2.1% to 4.0% for a poly(3-hexylthiophene) (P3HT):[6,6]-phenyl C_{61} butyric acid

* Corresponding author. Tel.: +82 2 450 3498; fax: +82 2 444 0765.
E-mail address: dkmoon@konkuk.ac.kr (D.K. Moon).

http://dx.doi.org/10.1016/j.jiec.2015.11.009
1226-086X/

methyl ester ($PC_{61}BM$)-based device by introducing LiF and BaF_2 between the cathode and active layer in a conventional structure. Sun et al. [18] reported that the efficiency was improved from 2.5% to 3.5% by introducing LiF on the ITO in an inverted structure.

However, because LiF or BaF_2 layer must be formed through vacuum deposition owing to the low solubility, the process becomes complicated, and the unit price increases. Lemmer et al. [19] reported the introduction of CsF with a high solubility in the alcohol-based solvent as an ETL. However, a P3HT:$PC_{61}BM$-based inverted-structure device exhibited a low efficiency (1.5%).

In this study, an inverted-structure device with a double interlayer (sol–gel zinc oxide (ZnO) layer + CsF layer formed through solution process) was fabricated. This device exhibited an efficiency of 8.2% after the electron mobility was enhanced by adding tunneling effects via metal fluoride.

Experimental

Materials

In both PTB7 and $PC_{71}BM$, 1-material products were acquired and used. A ZnO precursor was fabricated by performing hydrolysis at 50 °C for 12 h after dissolving 1 g of zinc acetate dihydrate ($Zn(CH_3COO)_2{\cdot}2(H_2O)$, 99.8%, Aldrich) and 0.28 g of monoethanolamine ($HOCH_2CH_2NH_2$, 99.5%, Aldrich) in 10 ml of 2-methoxyethanol ($(H_3CO)CH_2CHOH$, 99.8%, Aldrich) [20]. For an ETL, a solution obtained by dissolving CsF (99.9%, Acros) in isopropyl alcohol was used.

Device fabrication

First, the patterned ITO was sonicated in a detergent solution, isopropyl alcohol, and deionized water for 10 min each and cleaned. For dehydration, it was baked at 120 °C for 10 min. The ITO surface was treated for 20 min using an ultraviolet-ozone cleaner. A ZnO layer was formed after spin-coating the ZnO precursor solution on the cleaned ITO glass and annealing it at 150 °C. Then, an ETL was placed on the ZnO layer by spin-coating the CsF solution. To form a photoactive layer on the CsF layer, the devices were transported to a N_2-filled glove box. Then, a photoactive layer was formed by spin-coating a PTB7:$PC_{71}BM$ (1:1.5, w/w) in a chlorobenzene/1,8-diiodooctane (97:3, v/v) solution. Lastly, the anode was acquired by depositing 5 nm of MoO_3 and 100 nm of Ag in a high-vacuum chamber. The CsF layer was optimized by adjusting the concentration from 0.2 to 2 mg ml^{-1}.

Measurements

The current density–voltage (*J–V*) characteristics of the fabricated devices were measured using a Keithley 2400 source measurement unit and an AM 1.5G solar simulator (Oriel 96000 150 W solar simulator). In addition, the incident photon to current conversion efficiency (IPCE) was measured with respect to the optimized device and a reference. The thin films' surface morphology was measured using atomic force microscopy (AFM, PSIA XE-100, non-contact mode). To determine the changes in electron mobility through the CsF layer, an electron-only device was fabricated, and the electron mobility was measured using the space charge limited current (SCLC) method. Furthermore, to calculate the quenching rate of devices, the photoluminescence (PL) was measured using PerkinElmer LS55.

Results and discussion

Fig. 1 shows the structure of inverted devices (Fig. 1a), including the molecular structures of the donor PTB7 (Fig. 1b) and the acceptor $PC_{71}BM$ (Fig. 1c). In the device, a ZnO layer spin-coated with a ZnO precursor was formed [20]. Then, the ETL was placed on the ZnO layer by spin-coating the CsF solution. In the N_2-filled glove box, to form the photoactive layer, the mixed solution comprising PTB7 and $PC_{71}BM$ (1:1.5, w/w) was spin-coated. Finally, MoO_3 and Ag anodes were vacuum-deposited. The ETL was optimized by changing the concentration from 0.2 to 2 mg ml^{-1}.

Fig. 2 shows the *J–V* curves and IPCE spectra of the devices, and Table 1 summarizes the results. As Table 1 shows, a device with

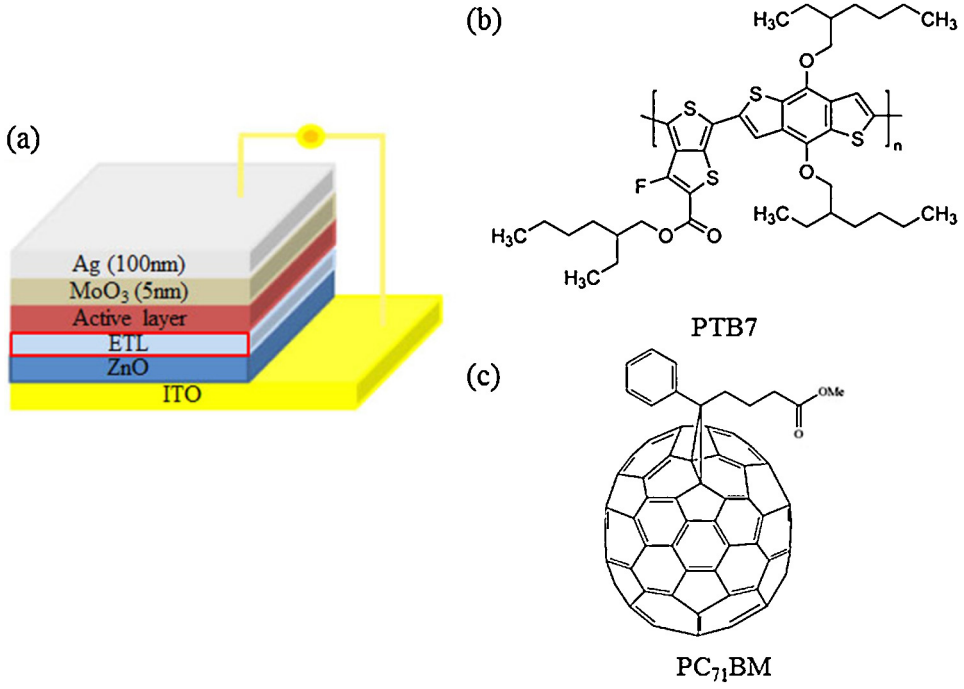

Fig. 1. (a) Structure of device introducing CsF layer and structures of (b) PTB7 and (c) $PC_{71}BM$.

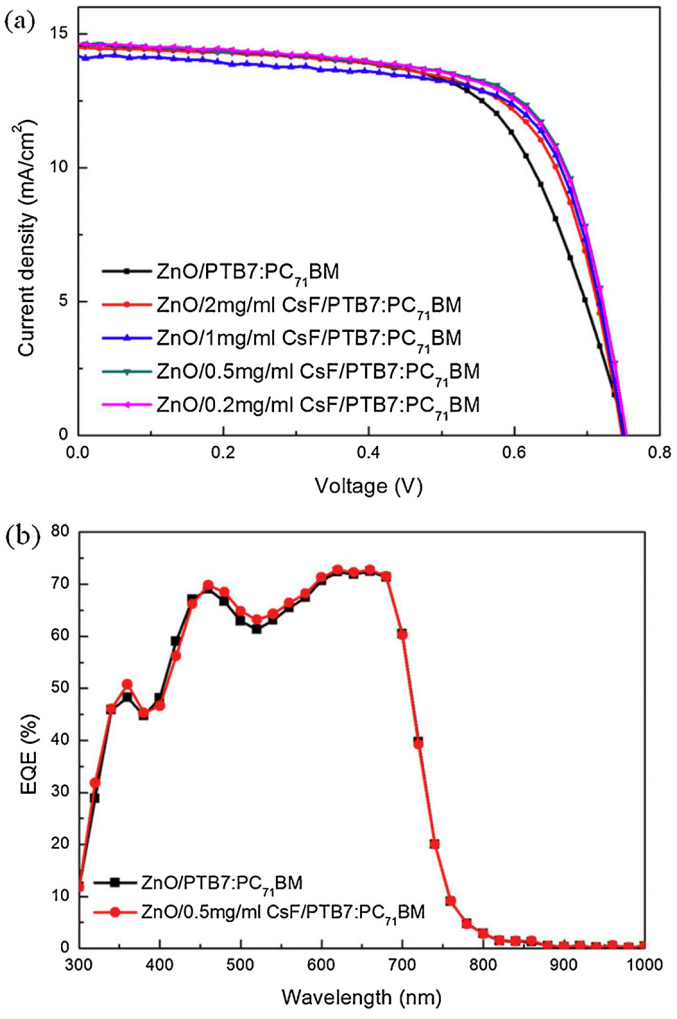

Fig. 2. (a) Current density–voltage (J–V) characteristics and (b) IPCE spectra of devices.

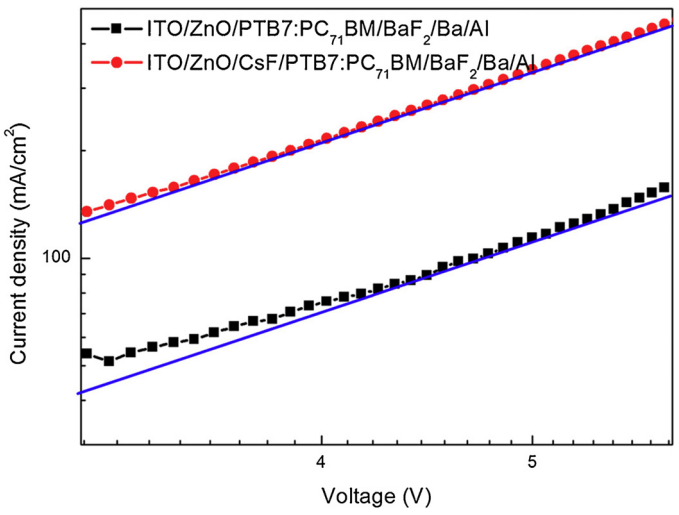

Fig. 3. Current density–voltage (J–V) characteristics of electron-only devices.

0.5 mg ml^{-1} CsF exhibited a V_{oc} of 0.757 V, a J_{SC} of 14.6 mA cm^{-2}, and a fill factor (FF) of 68.7%, yielding the highest PCE (8.2%). For the CsF-adopted device, the V_{OC} and J_{SC} were similar to those of the reference device (V_{OC} = 0.757 V, J_{SC} = 14.6 mA cm^{-2}, FF = 63.0%). In addition, similar external quantum efficiency was confirmed by the IPCE graph shown in Fig. 2b. However, as illustrated by the J–V curve shown in Fig. 2a, the FF increased by 9.3% from 63.0% to 68.7% in the CsF-adopted device because the introduction of the ETL decreased the series resistance (R_s) and increased the shunt resistance (R_{sh}). Therefore, in the device employing CsF as the ETL, the PCE was increased by 9.3% (η = 7.5% → η = 8.2%) by improving the device's FF without large changes in the V_{OC} and J_{SC}.

Fig. 3 shows the change in the internal resistance of devices corresponds to a decrease in the charge recombination by the improved transport characteristics of the electric charge separated from the photoactive layer. To measure the internal electron mobilities of devices, electron-only devices comprising ITO/ZnO/(CsF)/PTB7:$PC_{71}BM$/BaF_2/Ba/Al were fabricated, and the log J–log V plot is shown in Fig. 3. The electron mobilities were calculated using the Mott–Gurney Law (Eq. (1)) of SCLC theory, and the calculated data are summarized in Table 1 [21,22].

$$J = (9/8)\mu_e \epsilon_0 \epsilon_r (V^2/L^3) \quad (1)$$

J current density.
V applied voltage.
μ_e carrier mobility.
ε_0 dielectric constant of vacuum permittivity (8.85×10^{-14} F/cm).
ε_r dielectric constant of material (polymer = 3).
L active layer film thickness.

As stated in Table 1, the electron mobility of ZnO-based device was 7.46×10^{-3} cm^2/V s. When the CsF layer was adopted, the electron mobility was three times higher: 2.29×10^{-2} cm^2/V s. The electron mobility improved owing to the decrease in R_s and increase in R_{sh}; thus, the electron extraction—which represents the movements of the electron separated from the photoactive layer to external circuit through the electrode—increased [23].

Fig. 4 shows the surface morphology of the ITO/ZnO (Fig. 4a) and ITO/ZnO/CsF (Fig. 4b) structures, which was determined using AFM. As illustrated in Fig. 4, the root mean square (RMS) roughness of the ITO/ZnO/CsF surface (Fig. 4b, 1.783 nm) was greater than that of the ITO/ZnO surface (Fig. 4a, 1.649 nm). However, in the red-box region (enlarged image) of Fig. 4b, a value (1.614 nm) similar to the RMS roughness of the surface without CsF was observed. As the ETL-adopted CsF revealed in Scheme 1a, it was partially packed on the ZnO layer. In contrast to the part without CsF (Scheme 1b), the partially adopted CsF formed a dipole

Table 1
Characteristics of devices.

Device structure	V_{OC} (V)	J_{SC} (mA/cm^2)	FF (%)	PCE (%)	R_{sh} (Ω cm^2)	R_s (Ω cm^2)	Electron mobility (cm^2/V s)
ZnO/PTB7:$PC_{71}BM$	0.757	14.4 ± 0.2	62.5 ± 0.5	7.34 ± 0.17	1430	10.7	7.46×10^{-3}
ZnO/2 mg ml^{-1} CsF/PTB7:$PC_{71}BM$	0.757	14.4 ± 0.1	65.3 ± 1.0	7.66 ± 0.17	1469	7.1	–
ZnO/1 mg ml^{-1} CsF/PTB7:$PC_{71}BM$	0.757	14.2 ± 0.1	67.0 ± 1.4	7.75 ± 0.21	1500	6.9	–
ZnO/0.5 mg ml^{-1} CsF/PTB7:$PC_{71}BM$	0.757	14.5 ± 0.1	67.7 ± 1.0	7.99 ± 0.18	1530	6.1	2.29×10^{-2}
ZnO/0.2 mg ml^{-1} CsF/PTB7:$PC_{71}BM$	0.757	14.5 ± 0.1	66.6 ± 1.5	7.86 ± 0.23	1458	6.1	–

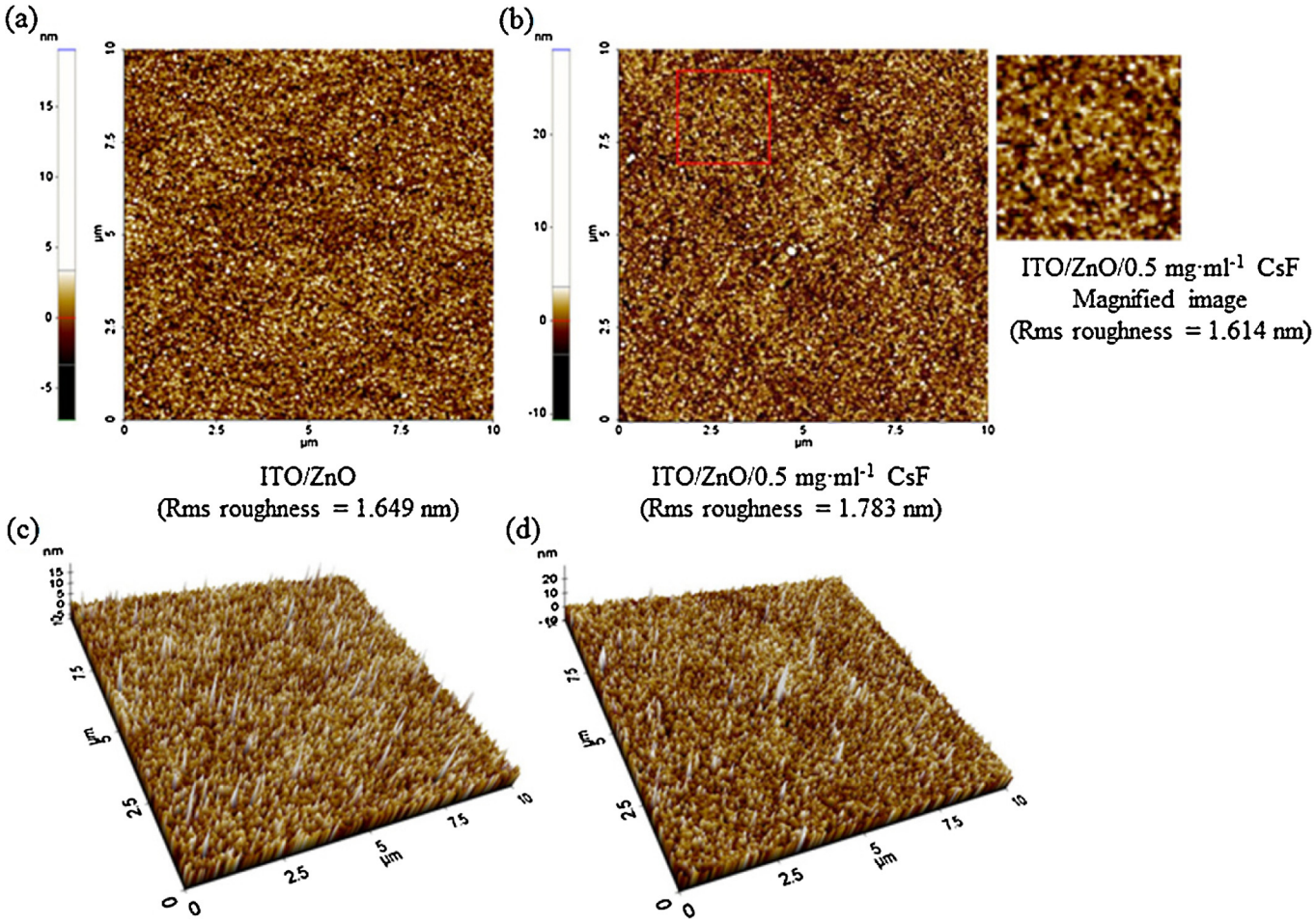

Fig. 4. AFM 2D topography of (a) ITO/ZnO and (b) ITO/ZnO/CsF with magnified image and 3D images of (c) ITO/ZnO and (d) ITO/ZnO/CsF.

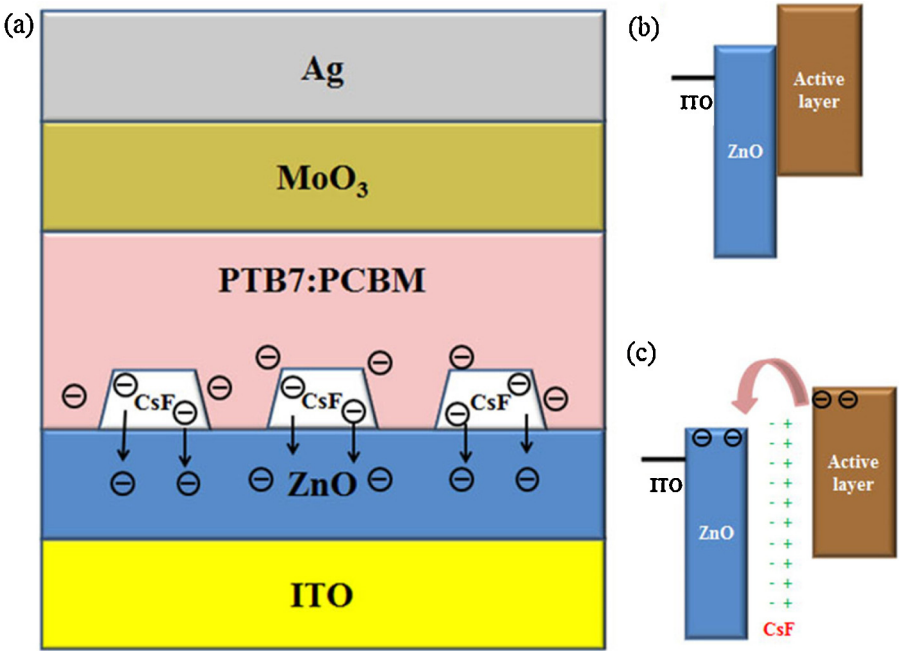

Scheme 1. Schematic images of electron transport mechanism.

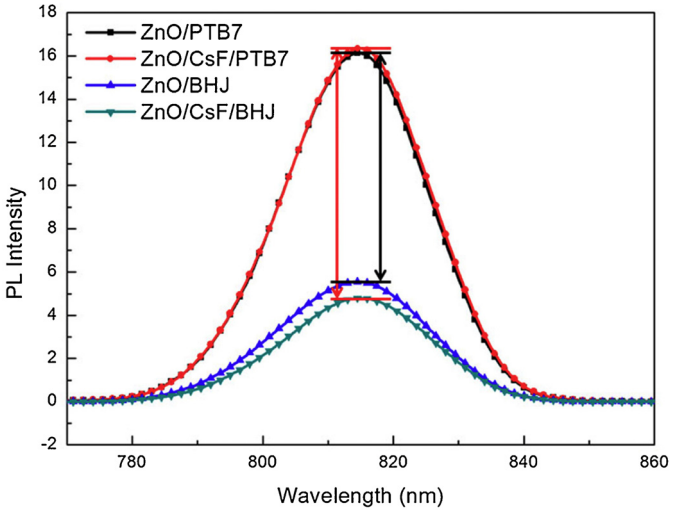

Fig. 5. PL intensity of various layers.

between the photoactive layer and ZnO (Scheme 1c). This dipole functioned as a tunnel site to create tunneling effects [17]. Thus, the introduction of CsF improves the electron extraction and reduces the electron–hole recombination by forming a tunnel site [23].

To verify the reduction of the electron–hole recombination, PL quenching data were obtained, as shown in Fig. 5. The difference in the PL spectrum between the donor polymer film and donor/acceptor blend BHJ film represents a quenched electron–hole. As the PL quenching rate increased, the recombination decreased through the efficient separation of the electrons and holes [23]. In the absence of $PC_{71}BM$ (acceptor), the PL intensity was slightly higher when CsF was adopted. Compared with the ZnO/BHJ film, the PL intensity was lower in a ZnO/CsF/BHJ film. According to our calculations, the PL quenching rates were 70.4% when the CsF layer was adopted. Therefore, they improved by 10% from the device without CsF layer(64.2%). The SCLC and PL quenching data indicate that the recombination of electron–hole separated from the photoactive layer decreased while the FF of the inverted PSCs increased owing to the efficient electron extraction.

Conclusion

We introduced inverted PSCs whose efficiency was enhanced through a double interlayer comprising a CsF layer on a ZnO layer. The partially formed CsF functioned as an electron tunnel to make the electrons move faster, yielding an improved electron mobility and a decreased recombination. With the improvement of the FF, the PCE reached 8.2%. Thus, we propose a method to improve the device efficiency and simplify the fabrication process by introducing a metal-fluoride layer with superior electron-transport capabilities through a solution process.

Acknowledgments

This paper was written as part of Konkuk University's research support program for its faculty on sabbatical leave in 2014 and by the National Research Foundation of Korea Grant funded by the Korean Government (MEST) (NRF-2012M1A2A2671703).

References

[1] S.W. Heo, K.H. Baek, H.J. Song, T.H. Lee, D.K. Moon, Macromol. Mater. Eng. 299 (2014) 353.
[2] Y. Sun, C. Cui, H. Wang, Y. Li, Adv. Energy Mater. 3 (2011) 1058.
[3] C. Yi, X. Hu, H.C. Liu, R. Hu, C.H. Hsu, J. Zheng, X. Gong, J. Mater. Chem. C 3 (2015) 26.
[4] I. Deckman, M. Moshonov, S. Obuchovsky, R. Brener, G.L. Frey, J. Mater. Chem. A 2 (2014) 16746.
[5] W. Yu, L. Huang, D. Yang, P. Fu, L. Zhou, J. Zhang, C. Li, J. Mater. Chem. A 3 (2015) 10660.
[6] S.H. Liao, H.J. Jhuo, Y.S. Cheng, S.A. Chen, Adv. Mater. 25 (2013) 4766.
[7] K. Zhao, L. Ye, W. Zhao, S. Zhang, H. Yao, B. Xu, M. Sun, J. Hou, J. Mater. Chem. C 3 (2015) 9565.
[8] M.H. Choi, K.W. Song, D.K. Moon, J.R. Haw, J. Ind. Eng. Chem. 29 (2015) 120.
[9] C.H. Hsieh, Y.J. Cheng, P.J. Li, C.H. Chen, M. Dubosc, R.M. Liang, C.S. Hsu, J. Am. Chem. Soc. 132 (2010) 4887.
[10] J. Subbiah, C.M. Amb, I. Irfan, Y. Gao, J.R. Reynolds, F. So, ACS Appl. Mater. Interfaces 4 (2012) 866.
[11] S.I. Na, T.S. Kim, S.H. Oh, J.K. Kim, S.S. Kim, D.Y. Kim, Appl. Phys. Lett. 97 (2010) 223305.
[12] H.S. Choi, J.S. Park, E.J. Jeong, G.H. Kim, B.R. Lee, S.O. Kim, M.H. Song, H.Y. Woo, J.Y. Kim, Adv. Mater. 23 (2011) 2759.
[13] Y. Zhu, X. Xu, L. Zhang, J. Chen, Y. Cao, Sol. Energy Mater. Sol. Cells 97 (2012) 83.
[14] Z. He, C. Zhong, S. Su, M. Xu, H. Wu, Y. Cao, Nat. Photo 6 (2012) 591.
[15] P. Cheng, J. Hou, Y. Li, X. Zhan, Adv. Energy Mater. 4 (2014) 1301349.
[16] K.G. Lim, M.R. Choi, J.H. Kim, D.H. Kim, G.H. Jung, Y.S. Park, J.L. Lee, T.W. Lee, ChemSusChem 7 (2014) 1125.
[17] J. Wang, F. Zhang, L. Li, Q. An, J. Zhang, W. Tang, F. Teng, Sol. Energy Mater. Sol. Cells 130 (2014) 15.
[18] Z. Lu, X. Chen, J. Zhou, Z. Jiang, S. Huang, F. Zhu, X. Piao, Z. Sun, Org. Electron. 17 (2015) 364.
[19] M. Reinhard, J. Hanisch, Z. Zhang, E. Ahlswede, A. Colsmann, U. Lemmer, Appl. Phys. Lett. 98 (2011) 053303.
[20] Y. Sun, J.H. Seo, C.J. Takacs, J. Seifter, A.J. Heeger, Adv. Mater. 23 (2011) 1679.
[21] P.N. Murgatroyd, J. Phys. D: Appl. Phys. 3 (1970) 151.
[22] T. Kirchartz, Beilstein J. Nanotechnol. 4 (2013) 180.
[23] S.W. Heo, E.J. Lee, K.W. Song, J.Y. Lee, D.K. Moon, Org. Electron. 14 (2013) 1931.